Reynolds Number Independence In An Urban Street Canyon Using 3D Robotic Particle Tracking Velocimetry

Dsouza, B.S.; Sciacchitano, A.

DOI
10.55037/lxlaser.21st.171

Publication date
2024

Document Version
Final published version

Published in
Proceedings of the 21st International Symposium on the Application of Laser and Imaging Techniques to Fluid Mechanics

Citation (APA)
Dsouza, B. S., & Sciacchitano, A. (2024). Reynolds Number Independence In An Urban Street Canyon Using 3D Robotic Particle Tracking Velocimetry. In *Proceedings of the 21st International Symposium on the Application of Laser and Imaging Techniques to Fluid Mechanics* Article 171 LISBON Simposia. https://doi.org/10.55037/lxlaser.21st.171

Reynolds Number Independence in an Urban Street Canyon using 3D Robotic Particle Tracking Velocimetry

B. Dsouza[1,*], A. Sciacchitano[1], W. Yu[1]

1: Faculty of Aerospace Engineering, Technische Universiteit Delft, The Netherlands
*Corresponding author: b.s.dsouza@tudelft.nl

Keywords: Urban Aerodynamics, Urban Canyon, Robotic PIV, Lagrangian Particle Tracking.

ABSTRACT

The Reynolds number in an Urban Street Canyon, $Re = U_{ref}H/\nu$ (U_{ref} is the velocity at $2H$, H is the building height, ν is the kinematic viscosity) is a difficult parameter to match between reduced-scale experiments and full-scale measurements. It is possible to overcome this mismatch in Reynolds numbers by satisfying the Reynolds number independence criterion, which states that above a certain critical Reynolds number, Re_c, the flow field remains invariant with increasing Reynolds numbers. For an urban canyon with an aspect ratio 1, this critical Reynolds number is often reported to be $Re_c = 12000$ for the mean flow quantities. This critical Reynolds number, however, is not applicable for higher-order quantities such as turbulence intensity and Reynolds stresses. In this study, 3D robotic particle tracking velocimetry was used to study the flow in an urban street canyon with an aspect ratio of 1 at several Reynolds numbers to estimate the critical Reynolds number for mean flow quantities and turbulence quantities. It was found that the critical Reynolds number for mean flow quantities was between $Re = 13000$ and $Re = 17000$. For the higher-order quantities, it was found that the critical Reynolds number was above 22000.

1. Introduction

An Urban Street Canyon is the space between two buildings. Urban canyon aerodynamics is important in the field of urban comfort and design because urban canyons have a poor self-ventilating capability and therefore tend to trap heat and pollutants (Chew et al. (2018); Britter & Hanna (2003)). In the context of experimental urban aerodynamics, the geometry of an urban street canyon is often simplified to rectangular blocks of length L, height H, and canyon width W. The aspect ratio of the canyon is defined as $AR = H/W$. Oke (1988) defines three different flow regimes within the Urban Canyon based on the aspect ratio. The worst-case scenario for the street canyon ventilation is the so-called skimming-flow regime, AR>0.65. In this scenario, there is a pronounced 'sheltering effect' resulting in high concentrations of pollutants at the pedestrian level (Li et al. (2006)). For canyons with L/W>7 and incoming wind perpendicular to the canyon

axis, the flow at the center plane of the canyon can be considered to be 2D, free from the 3D effects at the ends of the canyon (Hunter et al. (1990)).

The Reynolds number, $Re = U_{ref}H/\nu$ is an important parameter to determine if the flow is fully turbulent within the canyon, where U_{ref} is the reference velocity defined as the freestream velocity at height 2H from the canyon floor and ν is the kinematic viscosity of air. In wind tunnel experiments, the building height is of the order $10^{-2} - 10^{-1}$ m compared to full-scale field measurements with buildings of the order of 10^{1}m. The corresponding Reynolds numbers between the wind tunnel experiments and the field studies have a difference of 2 orders of magnitude (Table 1 from Chew et al. (2018)). This mismatch of Reynolds numbers can be justified by the Reynolds number independence hypothesis, which states that as long as the Reynolds number in the reduced-scale experiment exceeds a certain critical value Re_c, the normalized flow field remains invariant with increasing Reynolds numbers. There is, however, no clear agreement on the value of the critical Reynolds number. Chew et al. (2018) state that a generally acceptable critical Reynolds number is $Re_c \approx 12000$ for Urban Street Canyons with AR=1. They state that this value increases as the aspect ratio of the canyon is increased. For Canyons with AR=1, only a single stable vortex is observed for all Reynolds numbers tested ranging from reduced-scale tests at Re=1000 up to full-scale field studies at Re = $10^5 - 10^6$ (Caton et al. (2003); Kovar-Panskus et al. (2002); Meroney et al. (1996)). However, the critical Reynolds number mentioned in most of the literature is applicable only for mean flow quantities. There are relatively fewer studies analyzing turbulence quantities and higher-order statistics.

The goal of the present study is to confirm the range of the critical Reynolds number for an Urban Street Canyon in the skimming-flow regime and to estimate the critical Reynolds number for turbulence quantities in the 2D and 3D flow regions using 3D robotic Particle Tracking Velocimetry (3D-PTV).

2. Experimental Setup

2.1. Wind Tunnel Setup

The experiment was performed in an open circuit, open jet wind tunnel with a contraction ratio of 4:1 and an outlet cross-section of 60cm×60cm. A series of six simplified building models were mounted on an aluminium base-plate immediately downstream of the outlet. The experimental setup is presented in figure 1. To minimize reflections, the entire region illuminated by the laser is painted black. The first building is placed 500mm from the leading edge of the base-plate. All the canyons have an aspect ratio of 1. The canyon studied in the present experiment is in between

buildings 4 and 5 (figure 1b). The coordinate system of the canyon system is as follows: the x-axis is along the span of the canyon, the y-axis is pointing upwind, and the z-axis is oriented vertically. Reynolds numbers tested were $Re = 10000, 13000, 17000, 20000, 22000$, covering the ranges of the critical Reynolds number (Re_c) as reported in the literature (Shu et al. (2020); Chew et al. (2018)).

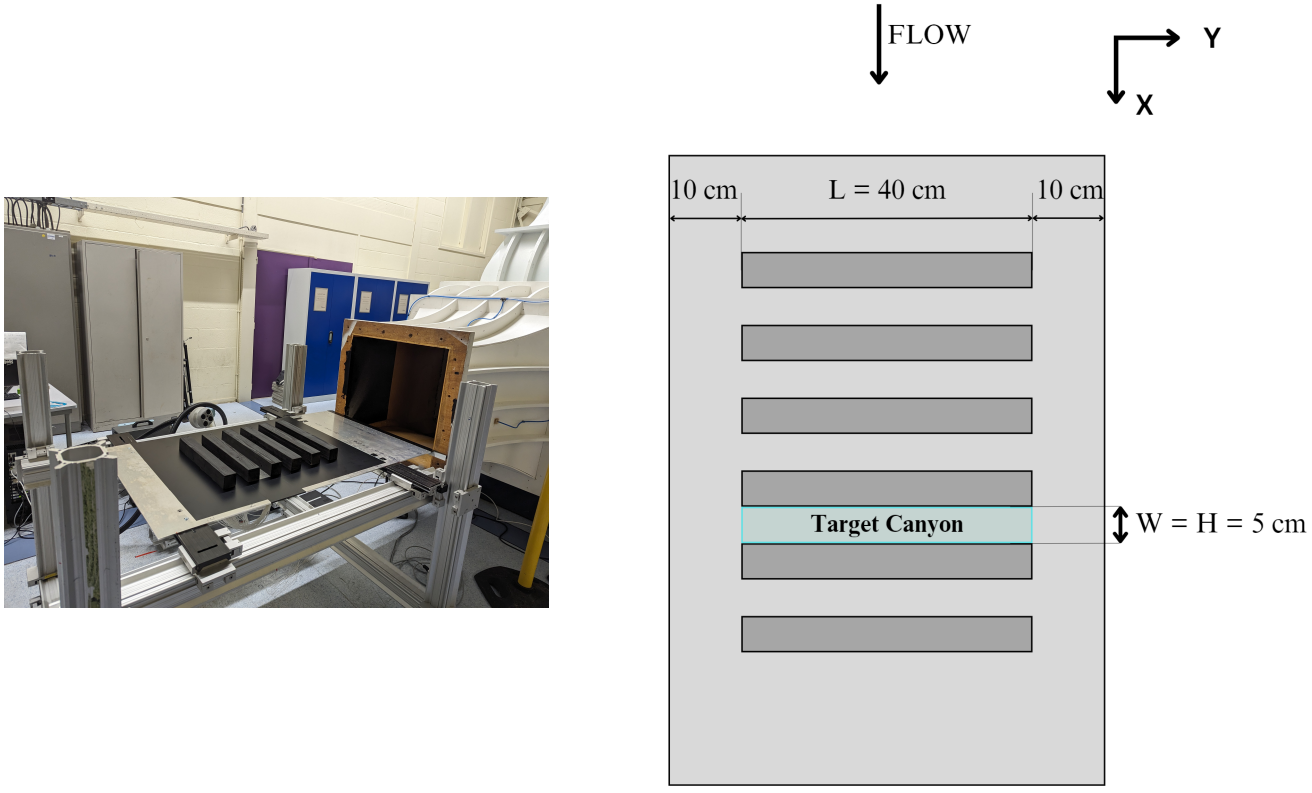

(a) Aluminium Base-plate and buildings

(b) Schematic of the Experiment

Figure 1. Experimental Setup

2.2. Measurement System

The PTV (Particle Tracking Velocimetry) setup is shown in figure 2. Helium-filled soap bubbles (HFSB) are used as high-intensity tracer particles in the wind tunnel test section. The HFSB seeding system consists of 200 nozzles arranged as 10 parallel wing rakes of 1m, each consisting of 20 nozzles spaced 5cm apart. The seeding surface area covers approximately 0.95×0.50 m^2. The bubble generator supplying the seeding rake is operated by a fluid supply unit (FSU), which controls the pressure of air, helium, and soap. The pressure is set and kept constant for the experiment. The pressures set were 2.0, 1.5, 2.0 bar for air, helium, and soap respectively. The nominal diameter of the tracer particles is $300\mu m$ with a maximum expected dispersion of $50\mu m$ (Kim et al. (2020); Faleiros et al. (2019)).

The Co-axial Volumetric Velocimetry (CVV) probe is mounted on a Universal Robots UR5 robotic arm with six degrees of freedom (3 rotations and 3 translations). The accuracy of translation of the robotic arm is $0.1mm$. The robotic arm is controlled using the software RoboDK. The software is used to program positions of the the CVV probe to capture images from different directions. The light source is a Quantronix Darwin Duo diode-pumped laser (λ = 527nm, 2$\times$25mJ pulse energy at 1kHz). An illustration of the Robotic PIV system is presented in figure 3.

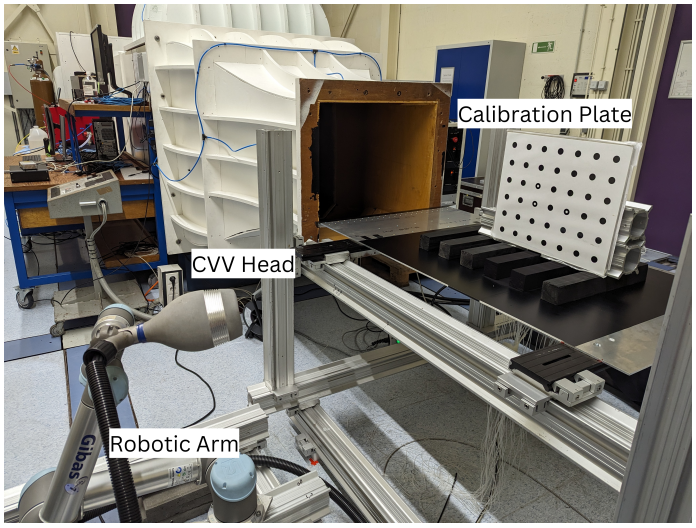

Figure 2. Robotic PIV System

The CVV probe consists of four CMOS cameras with 4mm objectives. The cameras are housed in an aerodynamic shell (LaVision Minishaker Aero). The laser light is transmitted via an optical fiber to the CVV head where the beam is expanded using a spherical lens. Table 1 tabulates the specifications of the CVV probe.

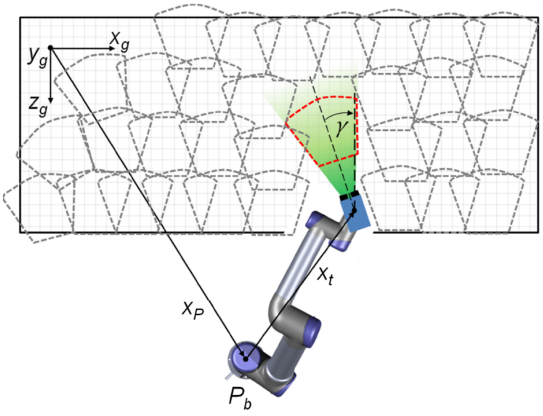

Figure 3. Illustration of the Robotic PIV system showing a global reference frame with an arbitrary region of interest (taken from Jux et al. (2018))

Table 1. Specifications of the CVV Probe

Optics	Focal Length	4mm
	Numerical Aperture	11
Imaging	Tomographic Aperture (at $z = 40cm$)	8° horizontal; 4° vertical
	Active Sensor	640×452 px^2 to 300×200 mm^2
	Pixel Pitch	4.8μm
	Magnification (at $z = 40cm$)	0.01
	Bit Depth	10
	Acquisition Frequency	727Hz
Illumination	Pulse Energy	25mJ
	Wavelength	527nm
	Spread Angle	40°

3. Results

This section discusses the results of the experiments. First, the analysis of the structure of the flow within the canyon will be presented for the baseline case with $Re = 10000$. Urban canyon flow is dominated by a stable vortex oriented along the canyon. For a long canyon (L/W>8), the flow around the central region of the canyon is dominated by this vortex. Figure 4 presents the streamwise velocity contours and vectors at various spanwise locations along the canyon. The development of the canyon vortex is clearly visible from the vector plot. At the edge of the canyon ($y/L = 0$), there is a strong positive streamwise velocity component over the entire height of the canyon because of the flow entering from the edge of the canyon. Moving further inwards into the canyon, a typical vortex structure is seen indicated by the reversal of flow in the lower half of the canyon. This region of re-circulation traps pollutants emitted at street level and prevents dispersion above the buildings. The canyon vortex is visualized using the λ_2 criterion in figure 6. In the following sections, the influence of Reynolds number on velocity profiles within this re-circulation region will be analyzed.

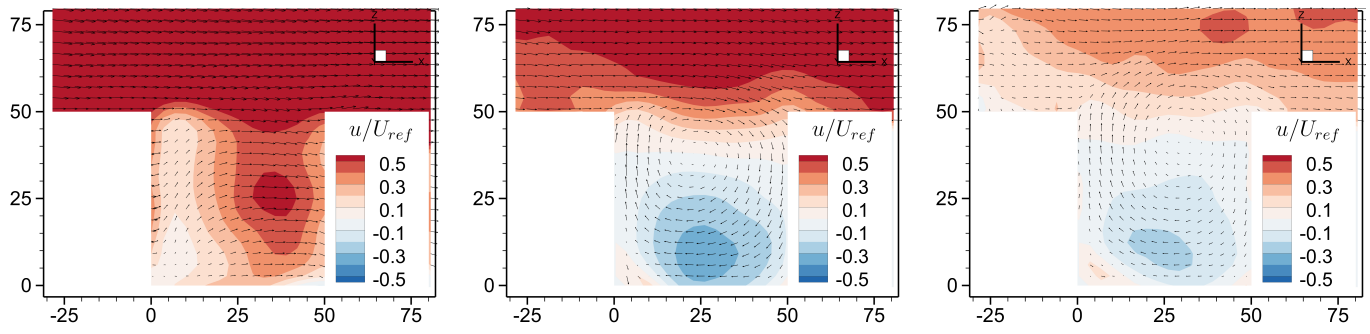

(a) $y/L = 0$ (b) $y/L = 0.125$ (c) $y/L = 0.25$

Figure 4. Streamwise Velocity

Towards the edges of the canyon, a second stable vortex exists, oriented vertically, introducing 3D flow features into the canyon as shown in figure 5. This vortex introduces 3D features within the canyon and is responsible for ventilating the canyon and dispersing pollutants. Figure 7 visualizes the canyon-end vortex with the λ_2 criterion.

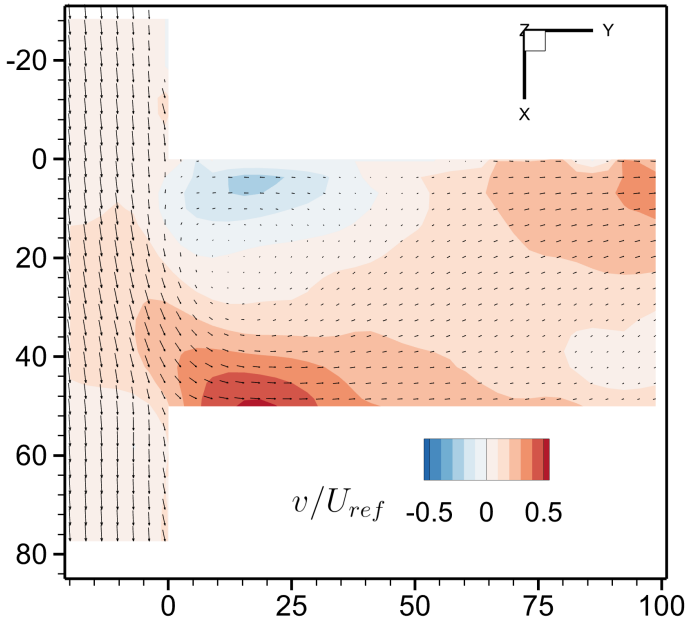

Figure 5. Lateral velocity contours at $z/H = 0.5$

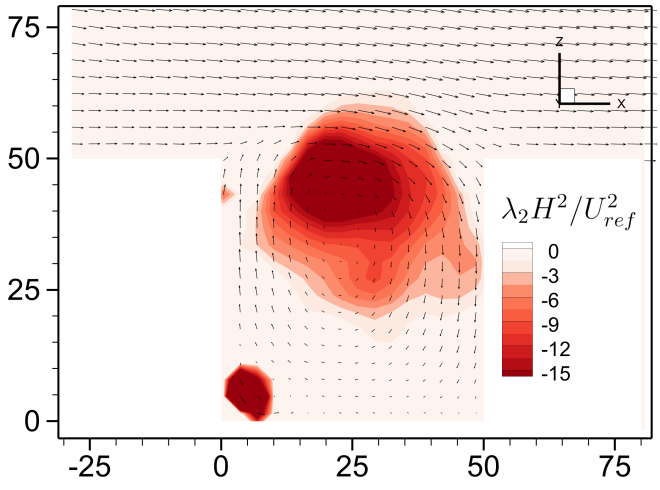

Figure 6. λ_2 contours at $y/L = 0.3$ showing a stable vortex

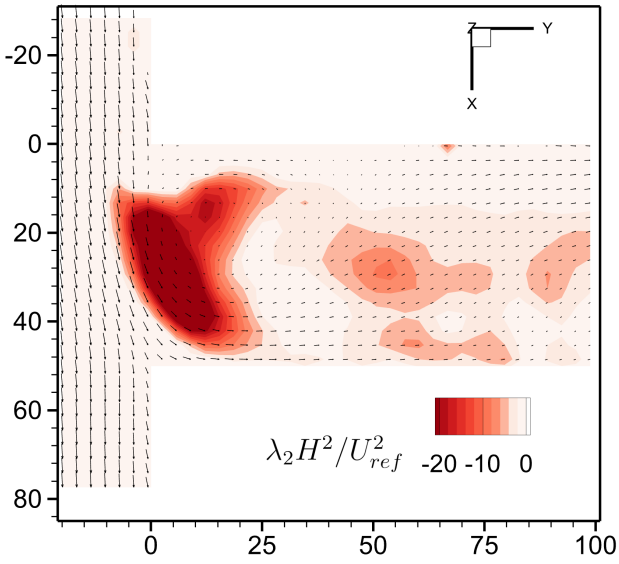

Figure 7. λ_2 contours at $z/H = 0.5$ showing a stable vertical vortex

3.1. Reynolds number effects

The following section analyzes Reynolds number effects in the urban street canyon for mean flow quantities and turbulence quantities.

3.1.1. Mean flow quantities

According to Chew et al. (2018), the critical Reynolds number for mean flow quantities is around $Re_c = 12000$. In this section, this critical value of Reynolds number will be assessed.

Figure 8 shows the streamwise velocity contours at $y/L = 0.3$ for Reynolds numbers ranging from $Re = 10000$ to $Re = 22000$. The overall structure of the flow is similar over the range of Reynolds numbers studied with no large-scale deviations in the flow field. The strength of flow reversal in the re-circulation region is the highest for the case of $Re = 10000$ and shows a decreasing trend and quickly converges for higher Reynolds numbers. Figures 8b, 8c, 8d, and 8e show very similar strengths of flow reversal in the re-circulation region. This is more evident from figure 10b and will be discussed further later in this section.

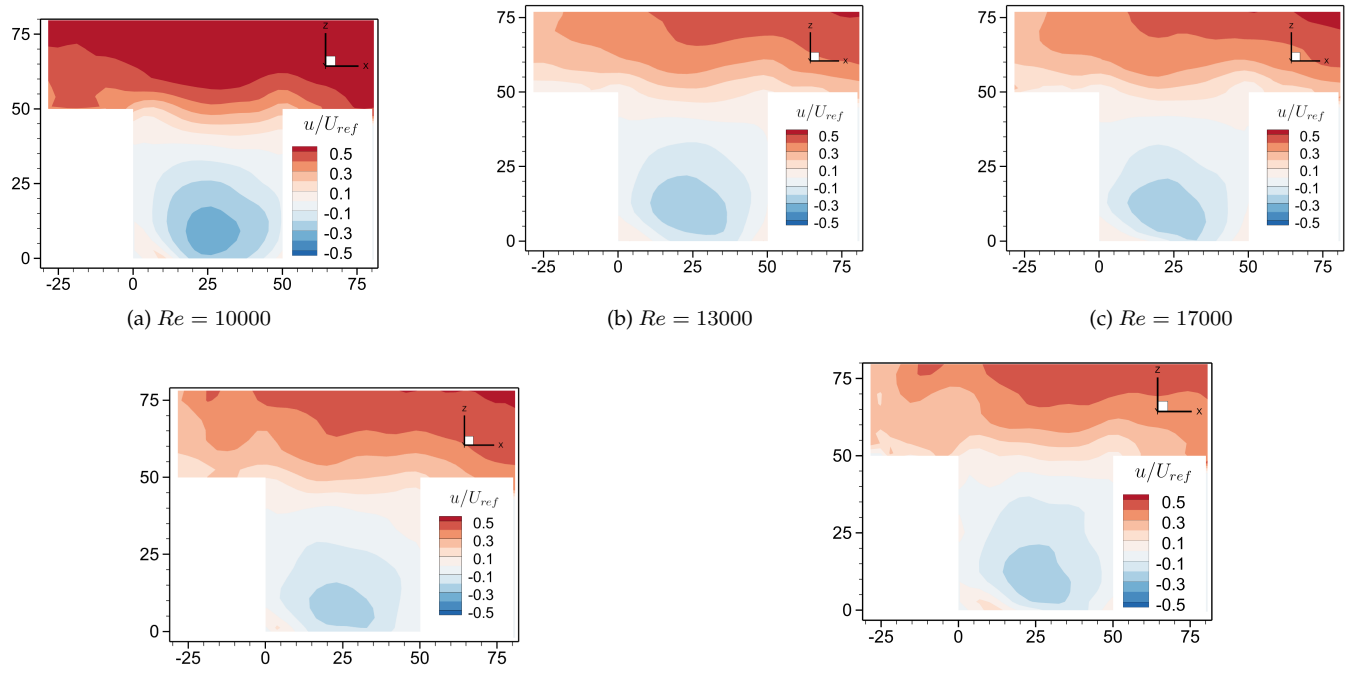

(a) $Re = 10000$ (b) $Re = 13000$ (c) $Re = 17000$

(d) $Re = 20000$ (e) $Re = 22000$

Figure 8. Contour plots of mean streamwise velocity u at $y/L = 0.3$

A similar pattern is observed in the contours of the vertical w-velocity field over the range of Reynolds numbers studied (see figure 9). The re-circulation region can be identified by the positive and negative peaks of w-velocity over the leeward and windward sides respectively. No significant structural differences are observed in all cases.

Velocity profiles along a vertical line at $z/H = 0.5$ are presented in figure 10. Reynolds number independence is achieved in the u-velocity field at $Re = 13000$ beyond which all normalized u-velocity profiles collapse on top of each other. For the lateral v-velocity field, Reynolds number independence is achieved between $Re = 13000$ and $Re = 17000$.The canyon exhibits a decreasing trend in spanwise velocities with increasing Reynolds numbers, primarily in the lower regions, and converge over $Re = 17000$.

The w-velocity profiles (see figure 10c) exhibit larger differences. However, since the overall magnitude of the w-velocity along the vertical profile is very low (5% of U_{ref}), these differences are not very significant compared to the mean freestream flow.

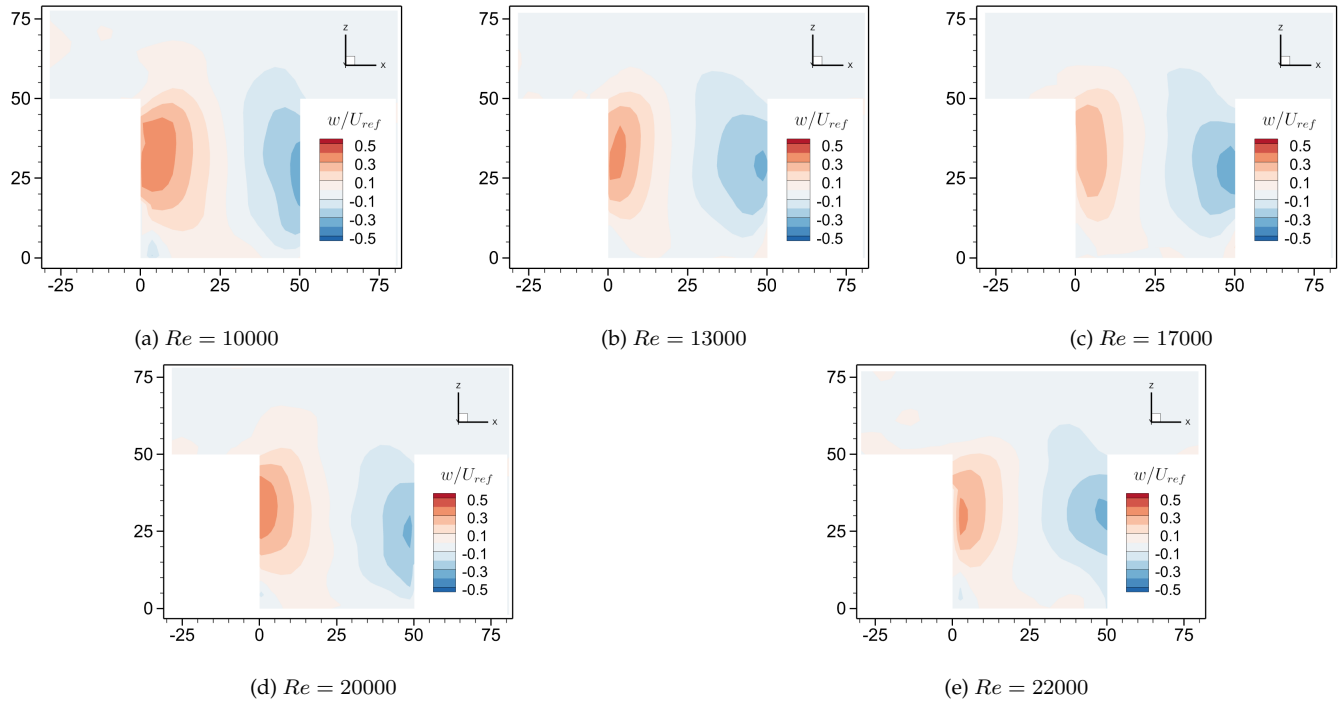

(a) $Re = 10000$ (b) $Re = 13000$ (c) $Re = 17000$

(d) $Re = 20000$ (e) $Re = 22000$

Figure 9. Contour plots of mean vertical velocity w at $y/L = 0.3$

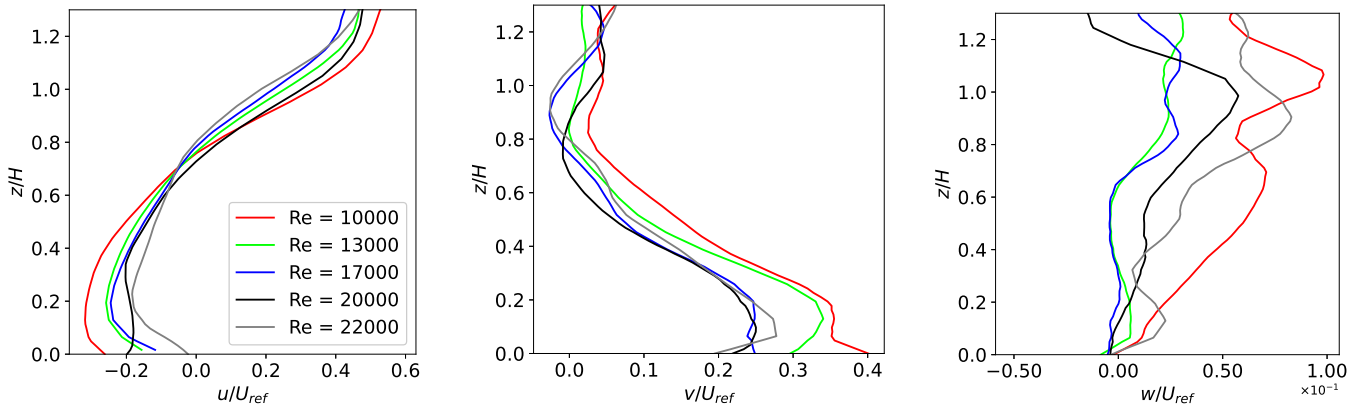

(a) u-velocity profiles at $x/L = 0.3$ (b) v-velocity profiles at $x/L = 0.3$ (c) w-velocity profiles at $x/L = 0.3$

Figure 10. Velocity profiles at $y/L = 0.3$ taken along a vertical line at $x/W = 0.5$

Overall, the canyon flow attains Reynolds number independence for all mean flow quantities between $Re = 13000$ and $Re = 17000$.

3.1.2. Turbulence Quantities

In this section, the Reynolds stresses will be analyzed for several Reynolds numbers to estimate the value of the critical Reynolds number. Figure 11 presents the Reynolds stress $\overline{u'u'}$. It is evident

from these plots that there are significant differences in the flow field with increasing Reynolds numbers. The intensity of $\overline{u'u'}$ shows a decreasing trend with increasing Reynolds numbers.

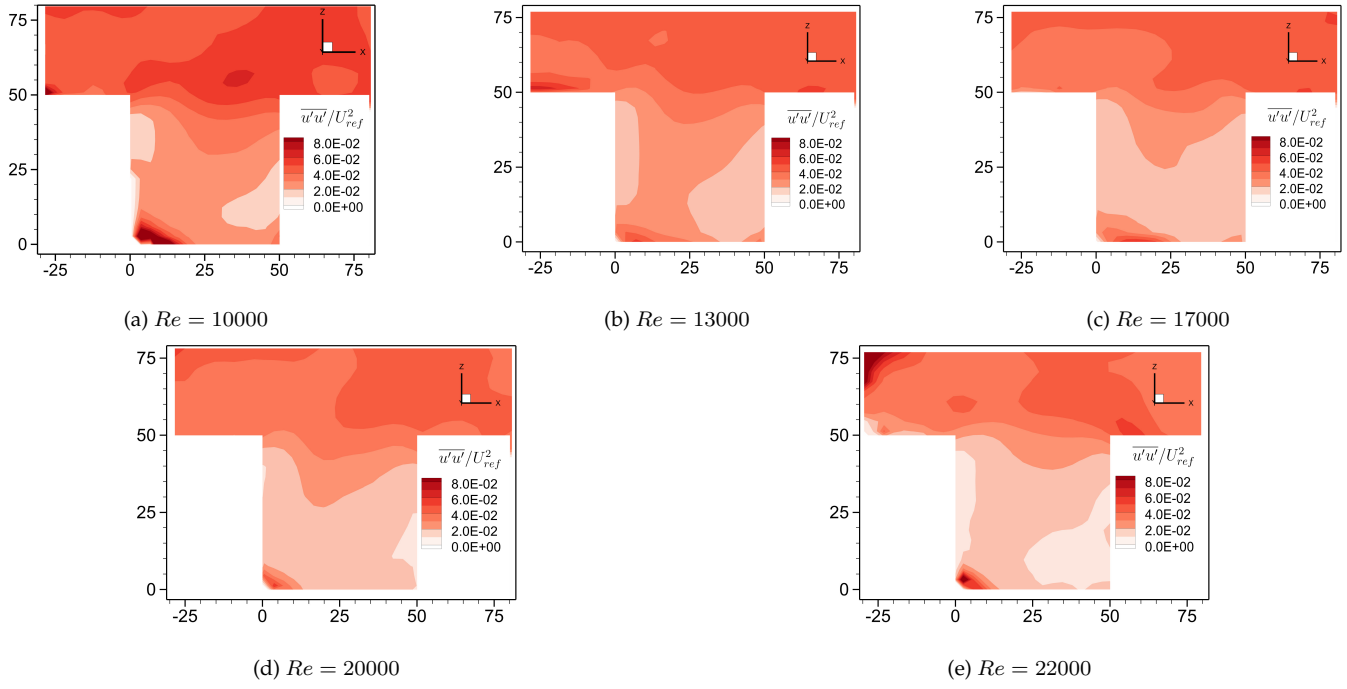

(a) $Re = 10000$ (b) $Re = 13000$ (c) $Re = 17000$

(d) $Re = 20000$ (e) $Re = 22000$

Figure 11. Contour plots of Reynolds stress $\overline{u'u'}$ at $y/L = 0.3$

Turbulence kinetic energy (TKE) contours are presented in figure 12. Similar to the Reynolds stresses, the TKE fields differ significantly with Reynolds numbers, with the intensity of TKE within the canyon reducing with increasing Reynolds numbers.

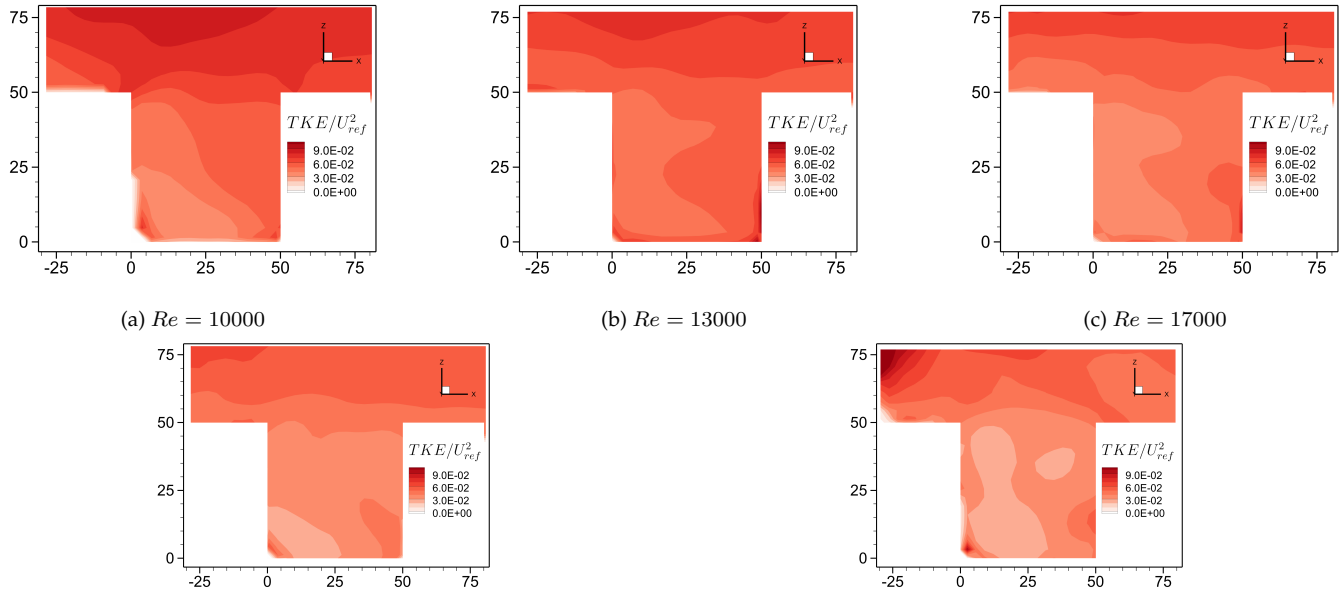

(a) $Re = 10000$ (b) $Re = 13000$ (c) $Re = 17000$

(d) $Re = 20000$ (e) $Re = 22000$

Figure 12. Contour plots of Turbulence Kinetic Energy at $y/L = 0.3$

Figure 13 presents a vertical profile of turbulence kinetic energy and Reynolds stress $\overline{u'u'}$ at $x/W = 0.5$ taken at $y/L = 0.3$. It is much clearer from these plots that the canyon flow does not attain Reynolds number independence within the range of Reynolds numbers tested. However, it can be observed that the profiles appear to converge towards a value with increasing Reynolds numbers. This is a strong indication that a critical Reynolds number exits for turbulence quantities, but is, however, higher than $Re = 22000$.

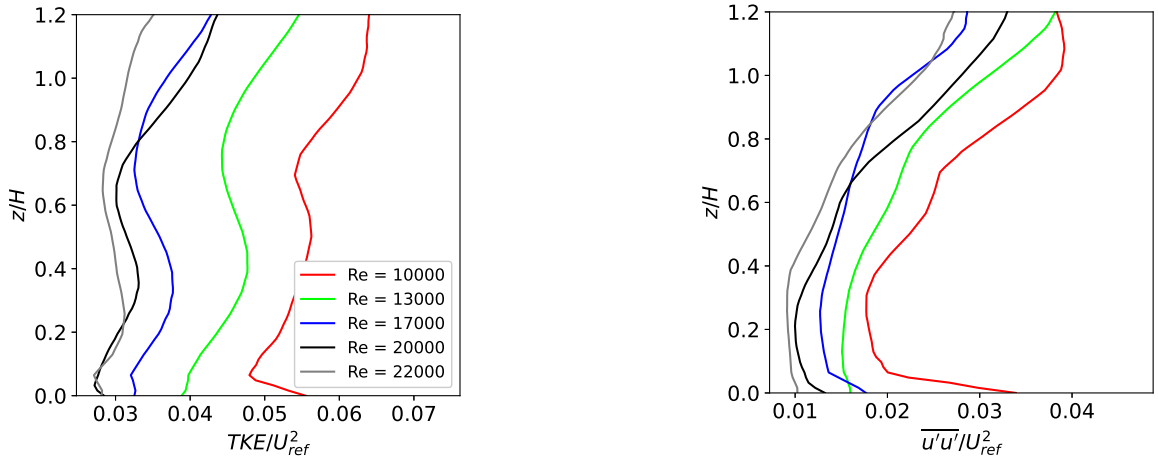

(a) Turbulence Kinetic Energy (b) Reynolds Stress $\overline{u'u'}$

Figure 13. TKE and Reynolds stress vertical profiles at $x/W = 0.5$ taken at $y/L = 0.3$

A similar pattern is observed in the horizontal profiles of TKE and $\overline{u'u'}$ at $z/H = 0.5$ taken at $y/L = 0.3$ (figure 14). The profiles appear to converge toward a value with increasing Reynolds numbers.

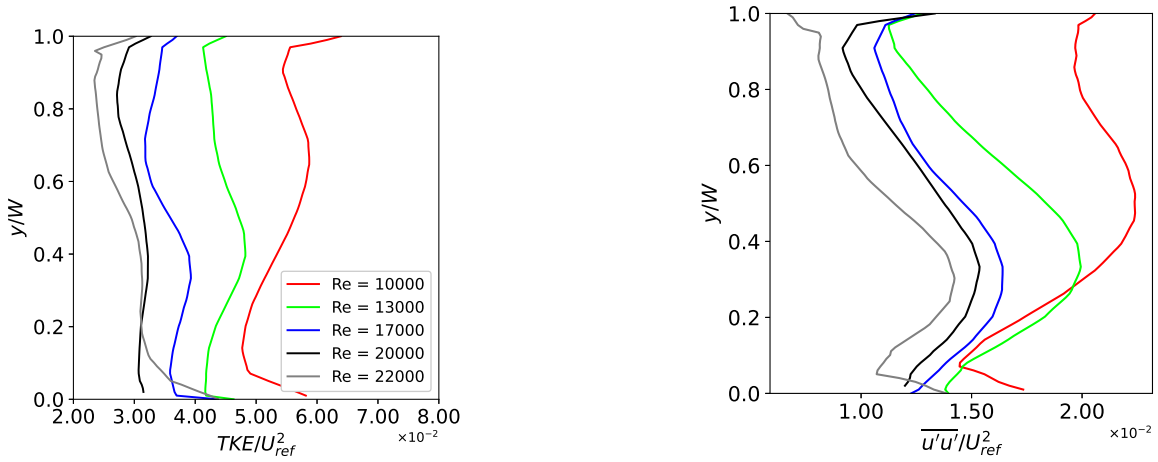

(a) Turbulence Kinetic Energy

(b) Reynolds Stress $\overline{u'u'}$

Figure 14. TKE and Reynolds stress horizontal profiles at $z/H = 0.5$ taken at $y/L = 0.3$

Because significant differences exist between the flow fields of turbulence quantities, the flow has not achieved Reynolds number independence within the range of Reynolds numbers tested. It is therefore necessary to perform the experiments reaching higher Reynolds numbers to be able to adequately assess the Reynolds number independence and estimate the critical Reynolds number for the turbulence quantities.

4. Conclusions

In this work, we attempt to estimate the critical Reynolds number for mean and turbulence quantities in an Urban Street Canyon with AR=1 using 3D robotic Particle Tracking Velocimetry. Reynolds numbers ranging from Re=10000 to Re=22000 were tested to estimate the critical Reynolds number for the mean flow quantities and for turbulence quantities. For the mean flow quantities, the normalized flow fields looked very similar for all Reynolds numbers, exhibiting only small differences in certain regions, such as near the top and bottom of the canyon, especially for the lower Reynolds numbers. Reynolds number independence was achieved for the mean velocities between Re=13000 and Re=17000. This value is a little bit higher than the results obtained by Chew et al. (2018). In contrast, for the turbulence quantities, such as the Turbulence Kinetic Energy (TKE) and the Reynolds stresses, significant differences were found in the flow field for all Reynolds numbers. It was not possible to estimate the critical Reynolds number for the turbulence quantities because this value seems to be higher than the range of Reynolds numbers tested in this study. A follow-up

experiment will be conducted exploring higher Reynolds numbers to arrive at an estimate for the critical Reynolds number for turbulence quantities.

Acknowledgements

The authors would like to acknowledge funding from the EU Horizon project TWEET-IE under Grant Agreement Number: 101079125.

Nomenclature

H	Height of the building [m]
L	Length of the building [m]
W	Width of the canyon [m]
Re	Reynolds number [-]
Re_c	Critical Reynolds number [-]
u	x velocity [m s^{-1}]
v	y velocity [m s^{-1}]
w	z velocity [m s^{-1}]
U_{ref}	Reference velocity at 2H [m s^{-1}]
V	Velocity magnitude [m s^{-1}]
ν	Kinematic Viscosity [m^2 $s-1$]

References

Britter, R. E., & Hanna, S. R. (2003). Flow and dispersion in urban areas. *Annual review of fluid mechanics*, *35*, 469–496.

Caton, F., Britter, R., & Dalziel, S. (2003). Dispersion mechanisms in a street canyon. *Atmospheric Environment*, *37*(5), 693–702.

Chew, L. W., Aliabadi, A. A., & Norford, L. K. (2018). Flows across high aspect ratio street canyons: Reynolds number independence revisited. *Environmental Fluid Mechanics*, *18*, 1275–1291.

Faleiros, D. E., Tuinstra, M., Sciacchitano, A., & Scarano, F. (2019). Generation and control of helium-filled soap bubbles for piv. *Experiments in Fluids*, *60*, 1–17.

Hunter, L. J., Watson, I., & Johnson, G. (1990). Modelling air flow regimes in urban canyons. *Energy and Buildings*, *15*(3-4), 315–324.

Jux, C., Sciacchitano, A., Schneiders, J. F., & Scarano, F. (2018). Robotic volumetric piv of a full-scale cyclist. *Experiments in Fluids*, *59*, 1–15.

Kim, D., Kim, M., Saredi, E., Scarano, F., & Kim, K. C. (2020). Robotic ptv study of the flow around automotive side-view mirror models. *Experimental Thermal and Fluid Science*, *119*, 110202. Retrieved from `https://www.sciencedirect.com/science/article/pii/S0894177720307068` doi: https://doi.org/10.1016/j.expthermflusci.2020.110202

Kovar-Panskus, A., Moulinneuf, L., Savory, E., Abdelqari, A., Sini, J.-F., Rosant, J.-M., ... Toy, N. (2002). A wind tunnel investigation of the influence of solar-induced wall-heating on the flow regime within a simulated urban street canyon. *Water, Air and Soil Pollution: Focus*, *2*, 555–571.

Li, X.-X., Liu, C.-H., Leung, D. Y., & Lam, K. M. (2006). Recent progress in cfd modelling of wind field and pollutant transport in street canyons. *Atmospheric Environment*, *40*(29), 5640–5658.

Meroney, R. N., Pavageau, M., Rafailidis, S., & Schatzmann, M. (1996). Study of line source characteristics for 2-d physical modelling of pollutant dispersion in street canyons. *Journal of wind Engineering and industrial Aerodynamics*, *62*(1), 37–56.

Oke, T. R. (1988). Street design and urban canopy layer climate. *Energy and buildings*, *11*(1-3), 103–113.

Shu, C., Wang, L. L., & Mortezazadeh, M. (2020). Dimensional analysis of reynolds independence and regional critical reynolds numbers for urban aerodynamics. *Journal of Wind Engineering and Industrial Aerodynamics*, *203*, 104232.